SCIENTIFIC REPORTS
nature research

OPEN

Influence of flicker noise and nonlinearity on the frequency spectrum of spin torque nano-oscillators

Steffen Wittrock[1]✉, Philippe Talatchian[1,2], Sumito Tsunegi[3], Denis Créte[1], Kay Yakushiji[3], Paolo Bortolotti[1], Ursula Ebels[4], Akio Fukushima[3], Hitoshi Kubota[3], Shinji Yuasa[3], Julie Grollier[1], Gilles Cibiel[5], Serge Galliou[6], Enrico Rubiola[6] & Vincent Cros[1]

The correlation of phase fluctuations in any type of oscillator fundamentally defines its spectral shape. However, in nonlinear oscillators, such as spin torque nano-oscillators, the frequency spectrum can become particularly complex. This is specifically true when not only considering thermal but also colored 1/*f* flicker noise processes, which are crucial in the context of the oscillator's long term stability. In this study, we address the frequency spectrum of spin torque oscillators in the regime of large-amplitude steady oscillations experimentally and as well theoretically. We particularly take both thermal and flicker noise into account. We perform a series of measurements of the phase noise and the spectrum on spin torque vortex oscillators, notably varying the measurement time duration. Furthermore, we develop the modelling of thermal and flicker noise in Thiele equation based simulations. We also derive the complete phase variance in the framework of the nonlinear auto-oscillator theory and deduce the actual frequency spectrum. We investigate its dependence on the measurement time duration and compare with the experimental results. Long term stability is important in several of the recent applicative developments of spin torque oscillators. This study brings some insights on how to better address this issue.

Spin torque nano-oscillators (STNOs) are nano-scale devices, which use spin polarized dc currents to drive a steady state electrical rf signal. Thereby, they exploit the spin transfer torque effect to excite the magnetization dynamics of a magnetic layer in a nanostructure. Those are converted into a dynamical change of the device resistance mapping the magnetic dynamics through the magnetoresistive effect existing in spintronic devices. Key property of STNOs is their nonlinearity, i.e. a coupling between the oscillator's amplitude and phase, which is an intrinsic effect of magnetic dynamics. Therefore, STNOs provide the unique opportunity for studying nonlinear dynamics at the nanoscale[1]. Furthermore, and also linked to their nonlinearity, they are considered as promising candidates for next-generation multifunctional spintronic devices[2,3]. In addition to their nano-metric size (∼ 100 nm), STNOs in general benefit from a high frequency tunability and compatibility with standard CMOS technology[4]. Potential applications are manifold and reach from high data transfer rate hard disk reading[5] and wide-band high-frequency communication[6–10] to spin wave generation[11,12] for e.g. magnonic devices[13,14]. More recently, STNOs have also been identified as key elements in the realization of broadband microwave energy harvesting[15] or frequency detection[16–18], and of reconstructing bio-inspired networks for neuromorphic computing[19,20]. All these functionalities, often realized in the very same STNO devices, are based

[1]Unité Mixte de Physique CNRS, Thales, Univ. Paris-Sud, Univ. Paris-Saclay, 1 Avenue Augustin Fresnel, 91767 Palaiseau, France. [2]Institute for Research in Electronics and Applied Physics, University of Maryland, College Park 20899-6202, MD, USA. [3]National Institute of Advanced Industrial Science and Technology (AIST), Spintronics Research Center, Tsukuba, Ibaraki 305-8568, Japan. [4]Univ. Grenoble Alpes, CEA, INAC-SPINTEC, CNRS, SPINTEC, 38000 Grenoble, France. [5]Centre National d'Études Spatiales (CNES), 18 av. Edouard Belin, 31401 Toulouse, France. [6]FEMTO-ST Institute, CNRS, Univ. Bourgogne Franche Comté, 25030 Besançon, France. ✉email: steffen.wittrock@cnrs-thales.fr

on basic spintronic phenomena, such as injection locking to an external rf signal[21,22], synchronization of multiple STNOs[23–26] or the spin torque diode effect[16,27–29].

Like any oscillator in nature, STNOs suffer from noise and their applicability in real practical devices must be measurable against their stability in terms of phase (or equivalently frequency). More specific to strongly nonlinear oscillators, such as STNOs, the amplitude noise must also be considered as it is converted into phase noise due to nonlinearity. In general, different mechanisms are found to govern the STNO's noise characteristics, usually expressed by its power spectral density (PSD). Principally, it includes thermal white noise processes, that dominate at higher offset frequencies from the carrier, and colored $1/f$ flicker noise processes, which dominate at low offset frequencies, i.e. at long timescales[30]. So far, especially thermal noise effects have been under consideration and were studied both experimentally[31,32] and theoretically[1,33,34]. It was found that the oscillator's nonlinearity strongly affects the noise PSD and the power emission frequency spectrum in the thermal regime. However, the understanding of colored $1/f$ flicker noise and its impact on the oscillation behaviour is still limited and usually relies on a phenomenological treatment[30] because of the noise's universality[35] and its potential manifold origins. Sources of $1/f$ noise might be intrinsic such as fluctuations of magnetization (for magnetic sensor devices[36–38]), the incidence of defects and/or inhomogeneities in the magnetic layers or the tunnel barrier notably due to the fabrication process[39]. Note that in addition to intrinsic origins, external fluctuations of the driving dc current or the applied magnetic field might also play a role. In experiments, the existence of $1/f$ noise at low offset frequencies has been reported in the different types of spin torque nano-oscillators based on the dynamics of a uniform magnetic mode[31,40], of the gyrotropic motion of a vortex core[30,32] or in nano-contact STNOs[39]. Keller *et al.* [40] have furthermore reported a different influence of the noise sources on the oscillation linewidth and spectral shape, related to the measurement duration. From the theoretical side, we have shown in a phenomenological model how the existence of both thermal noise and flicker noise is affecting the noise properties (phase and amplitude power spectral densities, PSDs) in the low offset frequency regime, and notably how the oscillator's nonlinearities play an important role[30].

In the present work, we investigate both theoretically and experimentally in vortex based spin transfer nano-oscillators (STVOs) how the presence of these different sources of noise, i.e. thermal and especially $1/f$ flicker noise, strongly impacts the main oscillations' characteristics, in particular their spectral shape. More specifically, we study how the oscillation's spectral shape depends on the measurement duration and distinguish the correlation times of the different noise sources. We demonstrate how the spectral shape changes from a Lorentz shape at short measurement durations associated to white noise correlation, to a Voigt—or even Gaussian—shape at longer durations with colored $1/f$ correlation, as similarly reported but not yet fully understood in Ref.[40]. In complement to these experimental results, we develop a simulation scheme including both a basic flicker noise process and thermal fluctuations. Finally, we furthermore present a theoretical model (see "Theoretical model" section) in which the variance functions of the phase fluctuations are derived allowing to predict the shape of the frequency spectrum of STVOs in particular, but generalizable to all types of STNOs[1,32,41].

Methods

Experiments. The experimental measurements presented in this work have been performed on vortex based spin transfer oscillators (STVOs). This type of STNOs exploits the gyrotropic motion of a magnetic vortex in a circular shaped nanodisk and converts its dynamics, which is sustained by spin transfer torque, into an electric rf signal due to the magnetoresistive effect[42]. Note that the occurrence of multiple modes as it is studied in Refs.[39,43] is particularly avoided here.

The studied samples consist of a pinned layer made of a conventional synthetic antiferromagnetic stack (SAF), a MgO tunnel barrier and a FeB free layer in a magnetic vortex configuration. The magnetoresistive ratio related to the tunnel magnetoresistance effect (TMR) lies around 100% at room temperature. The SAF is composed of PtMn(15)/$Co_{71}Fe_{29}$(2.5)/Ru(0.86)/CoFeB(1.6)/$Co_{70}Fe_{30}$(0.8) and the total layer stack is SAF/MgO(1)/FeB(4)/MgO(1)/Ta/Ru, with the nanometer layer thickness in brackets. The circular tunnel junctions have an actual diameter of $2R = 375$ nm. The presented experimental results have been recorded with an applied out-of-plane field of $\mu_0 H_\perp = 495$ mT, with μ_0 the vacuum permeability, and a dc current of $I_{dc} = 5.5$ mA. More details on the measurement techniques can be found in Ref.[30].

Simulation. We perform numerical simulations of the differential Thiele equation which describes the dynamics of the vortex core[44,45]:

$$\mathbf{G} \times \frac{d\mathbf{X}}{dt} - \hat{D}(\mathbf{X})\frac{d\mathbf{X}}{dt} - \frac{\partial W(\mathbf{X}, I_{\mathrm{STO}}(t))}{\partial \mathbf{X}} + \mathbf{F}^{STT}(\mathbf{X}, I_{\mathrm{STO}}(t)) = 0.$$

$\mathbf{X}$ denotes the vortex core position, $\mathbf{G}$ the gyrovector, $\hat{D}$ the damping, W the potential energy of the vortex, $\mathbf{F}^{STT}$ the spin-transfer force, and I_{STO} the applied dc current.

In this work, our objective is to include in the simulations both thermal and $1/f$ flicker noise. To do so, the contribution of the thermal noise is introduced through a fluctuating field varying the vortex core position[46]. It follows a normal distribution with a zero mean value and a fluctuation amplitude given by Γ:

$$\Gamma = \frac{2k_B T D_0}{R^2 G}, \tag{1}$$

where k_B is the Boltzmann constant, T corresponds to the temperature (set to 300 K in our simulations), D_0 is the linear (in the gyration amplitude) term of the damping force $\hat{D}$, R is the nano-dot radius and G is the amplitude

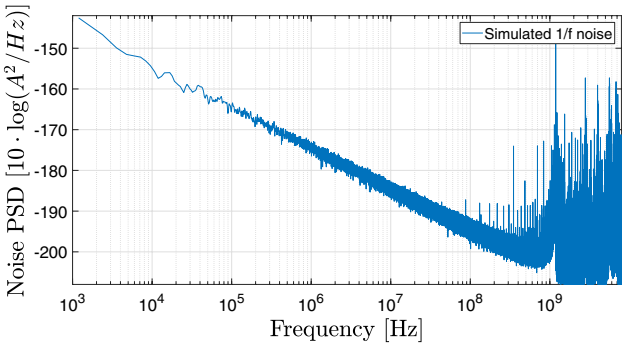

Figure 1. Modelled $1/f$ flicker noise PSD for the simulation, $\lambda = 2.5 \cdot 10^{-4}$. Fluctuations are added to the simulated dc current.

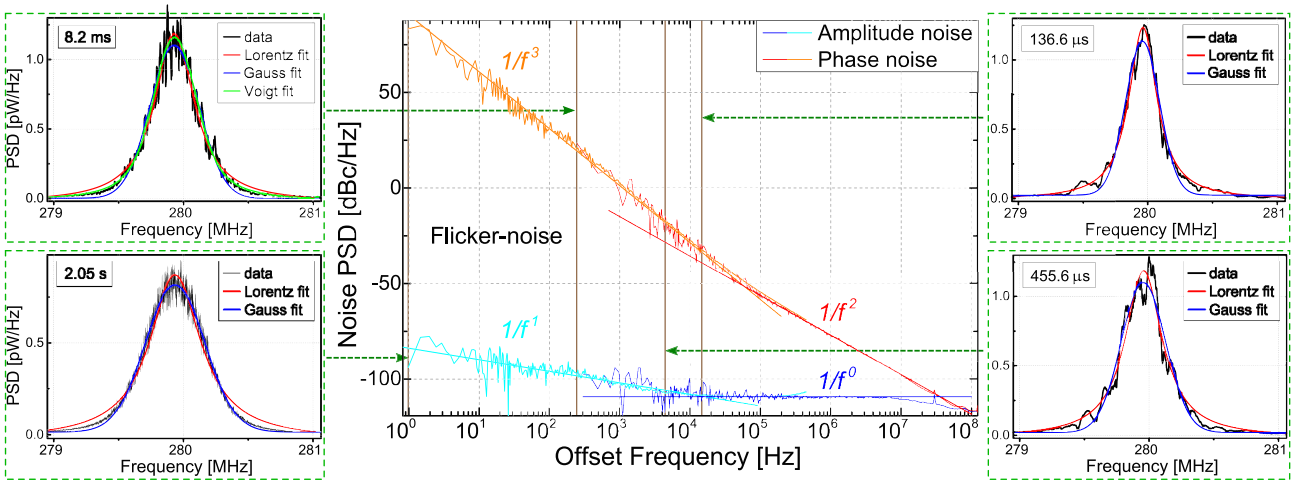

Figure 2. Measurement of amplitude and phase noise $S_{\delta\epsilon}$ and $S_{\delta\phi}$, respectively, and of frequency spectra corresponding to different measurement durations. $\mu_0 H_\perp = 495$ mT, $I = 5.5$ mA. The performed fits on the noise PSD show the characteristic $1/f^\beta$-behaviour for high (red, blue resp.) and low offset frequencies (orange, light blue resp.).

of the gyroforce **G**. The values of the parameters used in the explicit expression of the Thiele equation to simulate the vortex dynamics are given in the Supplementary Material[47].

As for the simulation of the flicker noise contribution, we introduce a random variable $r_{1/f}(t)$ that has a $1/f^1$ flicker noise PSD as presented in Fig. 1 (see Supplementary Material[47] for a more detailed description how this variable is constructed). This random process variable is then added to the applied dc current I_{dc} in order to model the flicker noise:

$$I_{STO}(t) = I_{dc} + \lambda r_{1/f}(t). \tag{2}$$

where λ is a scalar factor chosen here to be $2.5 \cdot 10^{-4}$ in order for the simulated amplitude and phase noise PSD to be close to measured ones but a little higher in order to clearly observe the effect of $1/f$ noise. Through I_{STO}, it consequently acts on the dynamics of both amplitude and phase. It is referred to the supplementary material[47] for a further discussion of the chosen modelling approach.

Experimental noise PSDs and frequency spectrum

In the central panel of Fig. 2, we present the measured noise PSD corresponding to amplitude (blue and cyan curves) and phase (red and orange curves) fluctuations. The different noise contributions can be directly identified due to their inverse power law behavior $PSD \sim 1/f^\beta$. At large offset frequencies $f \gtrsim 10^5$ Hz , the thermal noise is dominant and the noise signature behaves linearly with exponent $\beta = 2$ for the phase (red curve in Fig. 2) and $\beta = 0$ for the amplitude noise (blue curve in Fig. 2). Note that this description does not apply for frequencies above the relaxation rate frequency f_p (≈ 11.8 MHz here) above which the oscillator's nonlinearities strongly affect the noise PSDs[30,32,33].

At low offset frequency $f \lesssim 10^5$ Hz, the noise behaviors are clearly different because the flicker noise becomes the dominant source of noise. As seen in Fig. 2, the phase noise PSD can be fitted with α/f^3 (see orange curve in Fig. 2) and the amplitude noise with α/f^1 (see cyan curve in Fig. 2). In addition to the measured PSDs, we also

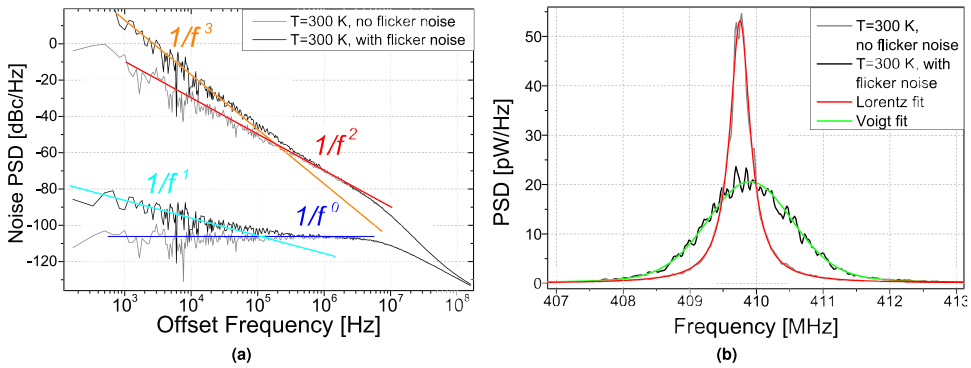

Figure 3. Simulation results with and without flicker noise. (**a**) Amplitude and phase noise PSD. (**b**) Corresponding frequency spectra.

present in Fig. 2 four frequency spectra recorded for different measurement times, i.e. $T_{mes} \triangleq 2/f = 136.6\,\mu s$, 456.6 µs, 8.2 ms and 2.05 s along with different fits on the measured spectra. We find that for short measurement times (typically < 1 ms), the power emission spectra can be fitted with an excellent agreement by Lorentzian curves. On the contrary, for longer measurement periods, the fits using Gaussian curves become more accurate with an excellent agreement for 2.05 s. In summary, we find a Lorentzian spectral shape in the regime of dominant thermal noise with the phase noise PSD $S_{\delta\phi} \sim 1/f^2$, and a Gaussian dominated shape in the regime of dominant flicker phase noise with $S_{\delta\phi} \sim 1/f^3$. Note that in the intermediate measurement time, the spectrum is described by a convolution of Lorentzian and Gaussian shapes, which is a Voigt curve shape, as exemplified for the 8.2 ms measurement time in Fig. 2.

In Fig. 3, we display the noise PSD (Fig. 3a) and the frequency spectrum (Fig. 3b) obtained from the simulation of the vortex core dynamics ("Simulation" section) using an applied dc current of 4.5 mA far enough from the critical current for auto-oscillations ~ 2 mA (thus, for the linewidth $2 \cdot \Delta f_0 \ll f_p$). To investigate the impact of $1/f$ flicker noise on the spectral shape of the STVOs, a sufficiently large simulation time scale of $T_{\mathrm{sim}} = 10$ ms is required. In Fig. 3a, we present two series of simulations, one with $\lambda = 2.5 \cdot 10^{-4}$ (i.e. including thermal and flicker noise) and another one with $\lambda = 0$ (i.e. including only thermal noise) [see Eq. (2)]. At large offset frequencies, $\gtrsim 0.2$ MHz, the simulated curves for the two λ are equivalent as expected because the flicker noise contribution is negligible in this regime. Below this offset frequency, the two curves separate. For $\lambda = 0$ and offsets $< f_p \simeq 8$ MHz, the noise PSD exhibits a plateau for the amplitude one and a $1/f^2$ decrease for the phase one. Note that in this case, despite the increase of phase noise due to amplitude-to-phase noise conversion associated to STNO nonlinearities[1,30–33], the noise PSD characteristics considering only thermal noise can be treated as that of a linear oscillator. For $\lambda = 2.5 \cdot 10^{-4}$ and offsets $< f_p \simeq 8$ MHz, the simulated PSDs show the same trends and characteristics as the experimental ones presented in Fig. 2, thus validating our approach to describe the flicker noise in the vortex dynamics simulations by assuming a $1/f^1$ generating noise process in the dynamical equations.

In Fig. 3b, we depict the corresponding frequency spectrum of the oscillation power. For $\lambda = 0$, the fit using a Lorentzian curve (red curve) shows a perfect agreement with the simulation. On the contrary, when the flicker noise is taken into account (using $\lambda = 2.5 \cdot 10^{-4}$), the spectrum becomes broader and its shape changes. The best fit is now obtained using a Voigt function (green curve), that is in fact close to be a Gaussian curve. We can thus conclude that the different noise sources contribute differently to the spectral shape of the oscillations. A direct consequence is that the spectral shape shall depend on the actual duration of the measurement as the flicker noise contribution becomes only significant at sufficiently large correlation times.

In Fig. 4, we plot the spectral linewidths of the according contributions (Lorentz, Gauss, Voigt) provided by the Voigt fits as a function of the duration both for the experimental spectra (Fig. 4a) and the simulated ones (Fig. 4b). Note that any difference between the two graphs, such as a larger linewidth in the simulation, is caused only by a slightly overestimated λ-parameter and simulation parameters (see supplementary[47]) which are not perfectly adapted to the specific sample characteristics, and do not qualitatively derogate the principal observation. That is, that we observe in these curve that the Lorentz contribution to the spectral linewidth does not change significantly with the recording time, whereas the total linewidth represented by the Voigt FWHM (*Full Width at Half Maximum*) increases for higher measurement time, as well as the contribution from the Gaussian shape.

Theoretical model

Taking into account both thermal and flicker noise processes within the framework of the general nonlinear auto-oscillator theory[1], the noise PSD of amplitude $S_{\delta\epsilon}$ and phase noise $S_{\delta\phi}$ can be written using the following expressions we recently described in[30]:

$$S_{\delta\epsilon} = \frac{\Delta f_0}{\pi} \cdot \frac{1}{f^2 + f_p^2} + \frac{1}{4p_0\pi^2\left(f_p^2 + f^2\right)} \cdot \frac{\alpha_{\delta\epsilon}}{f^\gamma} \tag{3}$$

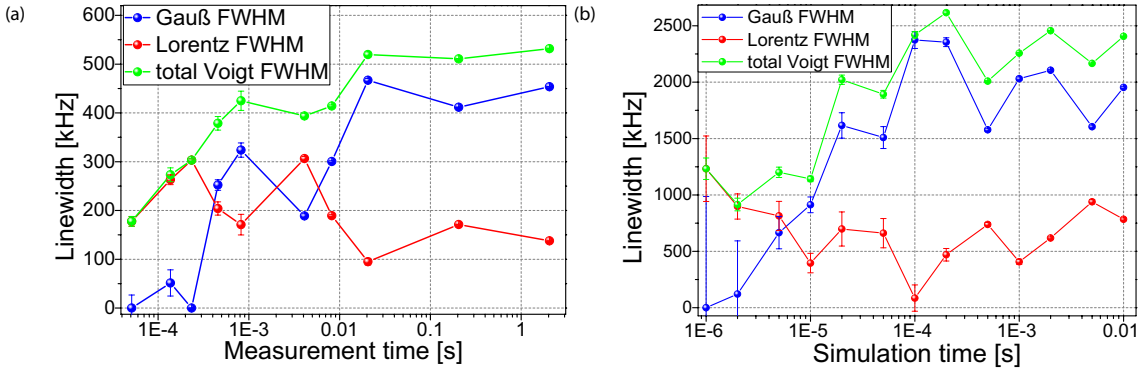

Figure 4. Resulting fit parameters from the Voigt fits for (**a**) the measurement and (**b**) the simulation. Next to the total Voigt linewidth, the linewidth corresponding to convoluted Lorentz and Gauß shape is shown.

$$S_{\delta\phi} = \frac{\Delta f_0}{\pi f^2} + \frac{1}{4p_0\pi^2 f^2} \cdot \frac{\alpha_{\delta\phi}}{f^\gamma} + \frac{\nu^2 f_p^2}{f^2} S_{\delta\epsilon}, \tag{4}$$

where Δf_0 is the linear oscillation linewidth and f_p is the characteristic frequency of relaxation back to the stable oscillation power p_0 after small perturbations δp. The parameter $\nu = Np_0/(\pi f_p)$ with $N = d\omega(p)/dp$ the nonlinear frequency shift coefficient is the normalized dimensionless nonlinear frequency shift and quantifies the coupling between phase and amplitude due to nonlinearity. The parameter $\alpha_{\delta x}$ describes the generating flicker noise process acting differently on amplitude/phase x. Its characteristic exponent γ has been found $\gamma = 1$.

In the following, we focus on the theoretical description of the phase noise $S_{\delta\phi}$, that is the most important for describing the spectral shape of the oscillation, which is one of the main objectives of this study. In Eq. (4), the three terms describe different contributions to the phase noise. The linear contributions are the ones being independent of ν, whereas the nonlinear ones are scaling with ν^2, converting amplitude $S_{\delta\epsilon}$ into phase noise $S_{\delta\phi}$. Moreover, all terms proportional to Δf_0 describe the thermal noise, and the terms proportional to $\alpha_{\delta x}$ the flicker noise contribution. For simplicity, we choose $S_{\delta\phi}$ to be expressed in terms of the angular frequency $\omega = 2\pi f$ and introduce the simplified parameters α_{ph} and α_{amp}. Thus in the following, we evaluate the phase noise in its simplified form:

$$\begin{aligned} S_{\delta\phi} = &\frac{2\Delta\omega_0}{\omega^2} + \nu^2 \frac{2\Delta\omega_0}{\omega^2} \frac{\omega_p^2}{(\omega^2 + \omega_p^2)} \\ &+ \frac{\alpha_{ph}}{\omega^3} + \frac{\alpha_{amp}}{(\omega_p^2 + \omega^2)\omega^3}. \end{aligned} \tag{5}$$

The parameters α_{ph} and α_{amp} can be identified with the experimental magnitudes:

$$\begin{aligned} \alpha_{\text{ph}} &= (2\pi)^3 \alpha_{\text{ph,exp}} = 2\pi\alpha_{\delta\phi}/p_0 \\ \alpha_{\text{amp}} &= (2\pi)^3 \omega_p^2 \alpha_{\text{amp,exp}} = 2\pi\omega_p^2 \nu^2 \alpha_{\delta\epsilon}/p_0, \end{aligned}$$

where $\alpha_{\text{amp,exp}}$ and $\alpha_{\text{ph,exp}}$ are the fitting parameters $\alpha_{x,\text{exp}}/f^3$ on the nonlinear low offset frequency flicker phase noise converted from amplitude noise [last term in Eq. (4)] and on the linear pure phase flicker noise [2nd term in (4)] respectively[30].

From Eq. (5), we can compute the variance of the oscillator's phase fluctuations[47–51] $\Delta\phi^2$:

$$\frac{\Delta\phi^2}{2} = \frac{1}{\pi} \int_0^\infty (1 - \cos(\omega t)) \cdot S_{\delta\phi} d\omega. \tag{6}$$

Assuming $S_{\delta\epsilon} \ll S_{\delta\phi}$ and a stationary ergodic process, which is gaussian distributed (via the central limit theorem), the signal's autocorrelation can be approximated by[47]:

$$K(t) \approx p_0 e^{-i\omega t} e^{-\Delta\phi^2/2}. \tag{7}$$

Then applying the Wiener-Khintchine theorem, the frequency spectrum's PSD of the signal x can be calculated through the Fourier transform of the signal's autocorrelation:

$$S_x(\omega) = \int_{\mathbb{R}} K_x(t) e^{i\omega t} dt. \tag{8}$$

Variance of phase fluctuations. Following the expression of Eq. (6) for the computation of the fluctuation's variance calculation, we first give the expression for the variance of the thermal noise contributions [all terms proportional to $\Delta\omega_0$ in Eq. (5)]:

$$\begin{aligned}\left(\frac{\Delta\phi^2}{2}\right)_{th} &\approx \frac{1}{\pi}\cdot\int_{\omega_c}^{\infty}(1-\cos(\omega t))S_{\delta\phi,th}d\omega \\ &= \frac{\alpha_l}{\pi\omega_c}+\frac{\alpha_l}{\pi}\cdot\left(\frac{t\pi}{2}-t\cdot\mathrm{Si}(t\omega_c)-\frac{\cos(\omega_c t)}{\omega_c}\right) \Big\}\text{linear part} \\ &+\frac{\alpha_{nl}}{\pi}\left(\frac{\omega_p+\omega_c\arctan(\frac{\omega_c}{\omega_p})}{\omega_c\omega_p^3}-\frac{\pi}{2\omega_p^3}\right) \\ &-\frac{\alpha_{nl}}{2\pi\omega_p^3}\big[\sinh(\omega_p t)\cdot\pi-\omega_p t\pi-\sinh(\omega_p t)\big(\mathrm{Si}(t(\omega_c+i\omega_p))+\mathrm{Si}(t(\omega_c-i\omega_p))\big) \\ &+i\cosh(\omega_p t)\big(\mathrm{Ci}(t(\omega_c+i\omega_p))-\mathrm{Ci}(t(\omega_c-i\omega_p))\big)-2\omega_p t\mathrm{Si}(t\omega_c)+\frac{2\omega_p\cos(t\omega_c)}{\omega_c}\big] \Big\}\text{nonlinear part,}\end{aligned}$$

where we insert for the linear thermal noise part $\alpha_l := 2\Delta\omega_0$ and $\alpha_{nl} := 2\Delta\omega_0\nu^2\omega_p^2$. $\mathrm{Si}(x)$ and $\mathrm{Ci}(x)$ denote the sine and cosine integral respectively, and ω_c is a lower frequency cutoff. For the two flicker noise terms, we calculate:

$$\begin{aligned}\left(\frac{\Delta\phi^2}{2}\right)_{1/f} &= \frac{\alpha_{ph}}{\pi}\left[\frac{1}{2\omega_c^2}+\frac{t^2}{2}\left(\frac{\sin(\omega_c t)}{t\omega_c}-\mathrm{Ci}(t\omega_c)-\frac{\cos(\omega_c t}{(\omega_c t)^2}\right)\right] \Big\}\text{pure flicker} \\ &+\frac{\alpha_{amp}}{\pi}\left[-\frac{\ln(\omega_p^2+\omega_c^2)}{2\omega_p^4}+\frac{1}{2\omega_c^2\omega_p^2}+\frac{\ln(\omega_c)}{\omega_p^4}\right] \\ &+\frac{\alpha_{amp}}{2\pi\omega_p^4}\Big[i\sinh(\omega_p t)\cdot[\mathrm{Si}(\omega_c t+i\omega_p t)-\mathrm{Si}(\omega_c t-i\omega_p t)] \\ &\quad+\cosh(\omega_p t)\cdot[\mathrm{Ci}(\omega_c t+i\omega_p t)+\mathrm{Ci}(\omega_c t-i\omega_p t)] \\ &\quad-\mathrm{Ci}(\omega_c t)\omega_p^2t^2-2\mathrm{Ci}(\omega_c t)+\frac{\omega_p^2t\sin(\omega_c t)}{\omega_c}-\frac{\omega_p^2\cos(\omega_c t)}{\omega_c^2}\Big] \Big\}\text{nonlinear flicker.}\end{aligned}$$

In all the calculation above, we have assumed a practical lower frequency cutoff ω_c, which is necessary to circumvent the integrals' divergence at $\omega = 0$. Note that for a comparative analysis of the timing jitter and frequency stability, the divergence is also often avoided by adding a filter function to Eq. (6)[51], invoking different variance definitions, as e.g. the Allan, modified Allan, or Hadamard variance[52]. However, it is to be emphasized that in real physical systems, our assumption will remain valid because the measurement time is usually restricted and the bandwidth is finite. In this sense, ω_c reflects the measurement duration studied in "Experimental noise PSDs and frequency spectrum" section. Moreover, the autocorrelation's delay t has to be limited, too, as $\omega_c t < 2\pi$. A reasonable approximation for the variance function is therefore $\omega_c t \ll 1$. Furthermore assuming $\omega_c \ll \omega_p$, we can approximate the above expressions. For the thermal noise part, with the analytical expressions for the prefactors $\alpha_l = 2\Delta\omega_0$ and $\alpha_{nl} = 2\Delta\omega_0\nu^2\omega_p^2$ introduced above, this gives:

$$\left(\frac{\Delta\phi^2}{2}\right)_{th} = \Delta\omega_0\left[(1+\nu^2)t-\nu^2\frac{1-e^{-\omega_p t}}{\omega_p}\right]. \tag{9}$$

This representation agrees with the one given by Tiberkevich *et al.* in Ref.[53], where also a detailed discussion of the temperature related effects in STNOs can be found. As the phase variance varies linearly only for time intervals $t \gg 2/\omega_p$, the STNO's power spectrum is thus in general non-Lorentzian. However, if the generation linewidth $\Delta\omega$ is sufficiently small, i.e. $2\Delta\omega \ll \omega_p$, the exponential factor in (9) can be neglected at a typical decoherence time $t \sim 1/\Delta\omega$:

$$\left(\frac{\Delta\phi^2}{2}\right)_{th} \approx \Delta\omega_0(1+\nu^2)t-\frac{\nu^2}{2\omega_p}.$$

This leads to a linear variance and thus, a Lorentzian power spectrum with a FWHM of:

$$\mathrm{FWHM} = 2\Delta\omega = 2\Delta\omega_0(1+\nu^2).$$

If the power fluctuations' correlation time holds $\tau_p = 2/\omega_p \gg 1/\Delta\omega$ and is therewith much longer than the oscillator's coherence time, Eq. (9) yields:

$$\left(\frac{\Delta\phi^2}{2}\right)_{th} \approx \Delta\omega_0\left(t+\frac{\nu^2\omega_p t^2}{2}\right),$$

which is quadratic and hence leads to a Gaussian power spectrum. However, in the case of large amplitude steady state oscillations of the STVO as investigated in this work, the condition $2\Delta\omega \ll \omega_p$ is always fulfilled. For the flicker noise, we obtain in approximation:

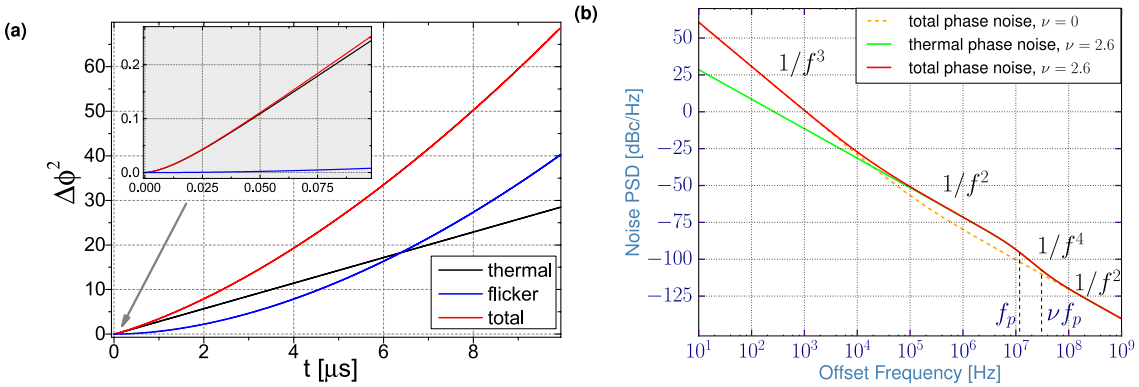

Figure 5. (**a**) Variance functions vs. time t. The inset shows the same functions at small times. (**b**) Corresponding phase noise PSD as a function of frequency offset. The curves named "total" include both thermal and flicker noise contributions.

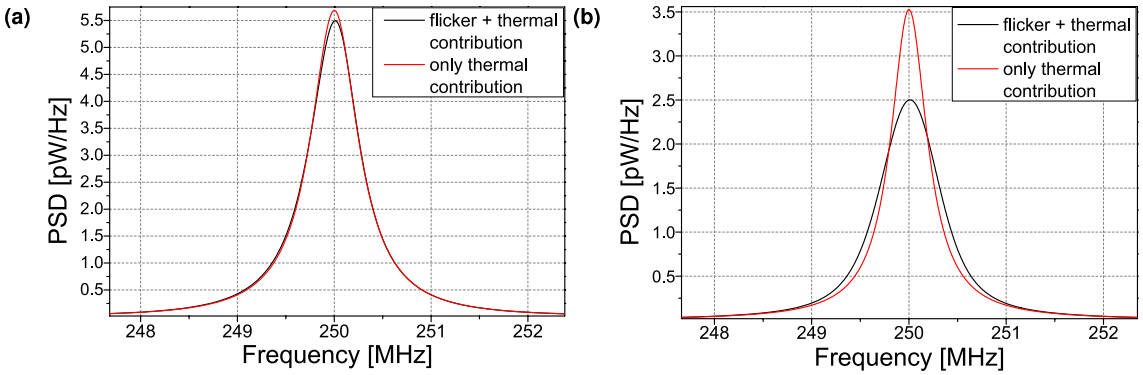

Figure 6. Calculated frequency spectra of the STNO signal with (**a**) $f_c = 10^5$ Hz and (**b**) $f_c = 1$ Hz.

$$\left(\frac{\Delta\phi^2}{2}\right)_{1/f} = \frac{\alpha_{ph}}{\pi}\frac{t^2}{2}\left[\frac{3}{2} - \ln(\omega_c t) - \gamma_{EM}\right] + \frac{\alpha_{amp}}{2\pi\omega_p^2}\left[\frac{\ln\left(\frac{\omega_c^2}{\omega_p^2}\right)}{2\omega_p^2} - \left(t^2 + \frac{2}{\omega_p^2}\right)(\ln(\omega_c t) + \gamma_{EM}) + 2t^2\right], \tag{10}$$

where we assume that $t \gg 2/\omega_p$ and introduce the Euler-Mascheroni constant $\gamma_{EM} \approx 0.58$.

In Fig. 5a, we plot the variance functions for the thermal and the flicker noise contributions using the experimental parameters of the STVO studied in "Experimental noise PSDs and frequency spectrum" section exhibiting a linewidth FWHM $= 2\Delta f_0 \cdot (1 + \nu^2) = 450$ kHz, a relaxation frequency $f_p = 11.8$ MHz, and a nonlinearity parameter $\nu = 2.6$. Corresponding to a standard measurement time, the frequency cutoff is set to $f_c = 500$ Hz. The fitting parameters of the linear and nonlinear flicker noise in the sample are $\alpha_{\mathrm{ph,exp}} = 1.15 \cdot 10^9$ and $\alpha_{\mathrm{amp,exp}} = 2.5 \cdot 10^7$ respectively.

At small times t, displayed in the inset of Fig. 5a, we clearly see that the thermal noise contribution (black curve) is the dominant one to the variance function. As already mentioned, this is nonlinear for very small times before it becomes almost linear for increasing t. However, at even higher t ($\gtrsim 7$ μs in Fig. 5a), because the flicker noise contribution starts to dominate, the total variance function becomes again nonlinear as the flicker variance appears to be almost quadratic.

In Fig. 5b, we plot the corresponding phase noise power spectral density based on Eq. (4). Similar to the noise PSD shown in "Experimental noise PSDs and frequency spectrum" section, we again emphasize the dominance of thermal noise at higher offset frequencies and of $1/f$ flicker noise at the lower ones ($f \lesssim 10^5$ Hz).

Theoretical frequency power spectrum. In Fig. 6, we present the calculated power spectrum using the expressions derived from the theoretical model. From the calculated variance $\Delta\phi^2$ of the phase fluctuations, we can determine the power spectrum according to eqs. (7) and (8).

As done for the simulations, we can now compare the theoretical spectral shape in the two cases i.e. only the thermal noise is considered or both thermal and flicker contributions are taken into account. For these calculations, we have used the same STVO parameters as before and only the frequency-cutoff f_c is changed. In Fig. 6a,

we observe that for $f_c = 10^5$ Hz (Fig. 6a), the spectrum is almost equivalent to the one only taking into account the thermal noise. In this case, the spectrum exhibits a Lorentzian shape due to its quasi-linear variance function $\Delta\phi^2$. On the contrary, for $f_c = 1$ Hz (Fig. 6b), corresponding to a longer measurement time, the two spectra clearly differ. While the spectral shape associated to pure thermal noise is, as expected, still of Lorentzian type, the power spectrum in the presence of flicker noise is more complex. As its variance function shown in Fig. 5a is nearly quadratic, we find a convolution of Lorentzian and Gaussian shapes, that is a Voigt function. This result obtained from the theoretical model thus reproduces excellently what we have previously shown both in the experiments and the simulations.

Conclusion

In this work, we measure the noise characteristics of vortex based spin torque oscillators and observe that they are dominated by thermal noise at large offset frequencies and by flicker noise mechanisms at lower ones $f \lesssim 10^5$ Hz. In order to analyze these results, we perform simulations of the oscillator's noise properties by including the thermal contribution and as well, more originally, the flicker noise processes existing in the vortex dynamics in STVOs. To this aim, we have used the differential Thiele approach[44] together with a $1/f^1$ shaped generated noise. An important outcome of the simulations is that the presence of a simulated flicker noise clearly modifies the actual spectral shape of the output signal. Being almost purely Lorentzian with only thermal noise, the spectral shape becomes rather Gaussian in the presence of flicker noise. This behavior is indeed precisely the one we observed experimentally by recording power spectra using different measurement times. These results are then corroborated to a theoretical model that we have developed applying the nonlinear auto-oscillator theory including not only thermal but also flicker noise processes. Doing so, we succeed to derive the complete phase fluctuation's variance function and in consequence the theoretical shape of the frequency spectrum. In complete agreement with both experiments and simulations, we find that because of the different noise type correlation times, the STNO's spectral shape indeed dependends on the measurement duration, being Lorentzian type on short time scales and becoming Voigt type at longer ones. We believe that these findings are especially important regarding the anticipated diverse applications of STNOs, particularly if frequency stability is required on long time scales. Moreover, because the approach used to described the influence of thermal and flicker noise in presence of nonlinearities is not restricted to the description of STNOs[1], the predictions made on the consequences on the spectral shape of the power spectra might also be valid for any other type of nonlinear oscillators that can be found in Nature.

Received: 4 December 2019; Accepted: 22 July 2020
Published online: 04 August 2020

References

1. Slavin, A. & Tiberkevich, V. Nonlinear auto-oscillator theory of microwave generation by spin-polarized current. *IEEE Trans. Magn.* **45**, 1875–1918 (2009).
2. Locatelli, N., Cros, V. & Grollier, J. Spin-torque building blocks. *Nat. Mater.* **13**, 11–20. https://doi.org/10.1038/nmat3823 (2013).
3. Ebels, U. *et al.* Spintronic based RF components. In *2017 Joint Conference of the European Frequency and Time Forum and IEEE International Frequency Control Symposium (EFTF/IFC)* (IEEE, 2017).
4. Kreißig, M. *et al.* Hybrid PLL system for spin torque oscillators utilizing custom ICs in 0.18 µm BiCMOS. In *2017 IEEE 60th International Midwest Symposium on Circuits and Systems (MWSCAS)* (IEEE, 2017).
5. Sato, R., Kudo, K., Nagasawa, T., Suto, H. & Mizushima, K. Simulations and experiments toward high-data-transfer-rate readers composed of a spin-torque oscillator. *IEEE Trans. Magn.* **48**, 1758–1764 (2012).
6. Muduli, P. K. *et al.* Nonlinear frequency and amplitude modulation of a nanocontact-based spin-torque oscillator. *Phys. Rev. B* **81**, 140408 (2010).
7. Choi, H. S. *et al.* Spin nano-oscillator-based wireless communication. *Sci. Rep.* **4**, 5486 (2014).
8. Purbawati, A., Garcia-Sanchez, F., Buda-Prejbeanu, L. D. & Ebels, U. Enhanced modulation rates via field modulation in spin torque nano-oscillators. *Appl. Phys. Lett.* **108**, 122402 (2016).
9. Ruiz-Calaforra, A. *et al.* Frequency shift keying by current modulation in a MTJ-based STNO with high data rate. *Appl. Phys. Lett.* **111**, 082401 (2017).
10. Litvinenko, A. *et al.* Analog and digital phase modulation of spin torque nano-oscillators. arXiv:1905.02443v1.
11. Demidov, V. E., Urazhdin, S. & Demokritov, S. O. Direct observation and mapping of spin waves emitted by spin-torque nano-oscillators. *Nat. Mater.* **9**, 984–988 (2010).
12. Madami, M. *et al.* Direct observation of a propagating spin wave induced by spin-transfer torque. *Nat. Nanotechnol.* **6**, 635–638 (2011).
13. Kruglyak, V. V., Demokritov, S. O. & Grundler, D. Magnonics. *J. Phys. D Appl. Phys.* **43**, 264001 (2010).
14. Chumak, A. V., Serga, A. A. & Hillebrands, B. Magnonic crystals for data processing. *J. Phys. D Appl. Phys.* **50**, 244001 (2017).
15. Fang, B. *et al.* Experimental demonstration of spintronic broadband microwave detectors and their capability for powering nanodevices. *Phys. Rev. Appl.* **11**, 014022 (2019).
16. Jenkins, A. S. *et al.* Spin-torque resonant expulsion of the vortex core for an efficient radiofrequency detection scheme. *Nat. Nanotechnol.* **11**, 360–364 (2016).
17. Louis, S. *et al.* Low power microwave signal detection with a spin-torque nano-oscillator in the active self-oscillating regime. *IEEE Trans. Magn.* **53**, 1–4 (2017).
18. Louis, S. *et al.* Ultra-fast wide band spectrum analyzer based on a rapidly tuned spin-torque nano-oscillator. *Appl. Phys. Lett.* **113**, 112401 (2018).
19. Torrejon, J. *et al.* Neuromorphic computing with nanoscale spintronic oscillators. *Nature* **547**, 428–431 (2017).
20. Romera, M. *et al.* Vowel recognition with four coupled spin-torque nano-oscillators. *Nature*https://doi.org/10.1038/s41586-018-0632-y *(2018).*
21. Lebrun, R. *et al.* Understanding of phase noise squeezing under fractional synchronization of a nonlinear spin transfer vortex oscillator. *Phys. Rev. Lett.* **115**, 017201. https://doi.org/10.1103/PhysRevLett.115.017201 (2015).
22. Hamadeh, A. *et al.* Perfect and robust phase-locking of a spin transfer vortex nano-oscillator to an external microwave source. *Appl. Phys. Lett.* **104**, 022408. https://doi.org/10.1063/1.4862326 (2014).

23. Kaka, S. *et al.* Mutual phase-locking of microwave spin torque nano-oscillators. *Nature* **437**, 389–392 (2005).
24. Locatelli, N. *et al.* Efficient synchronization of dipolarly coupled vortex-based spin transfer nano-oscillators. *Sci. Rep.* **5**, 17039 (2015).
25. Lebrun, R. *et al.* Mutual synchronization of spin torque nano-oscillators through a long-range and tunable electrical coupling scheme. *Nat. Commun.* **8**, 15825 (2017).
26. Tsunegi, S. *et al.* Scaling up electrically synchronized spin torque oscillator networks. *Sci. Rep.* **8**, 13475 (2018).
27. Tulapurkar, A. A. *et al.* Spin-torque diode effect in magnetic tunnel junctions. *Nature* **438**, 339–342 (2005).
28. Miwa, S. *et al.* Highly sensitive nanoscale spin-torque diode. *Nat. Mater.* **13**, 50–56 (2013).
29. Naganuma, H. *et al.* Electrical detection of millimeter-waves by magnetic tunnel junctions using perpendicular magnetized L10-FePd free layer. *Nano Lett.* **15**, 623–628 (2015).
30. Wittrock, S. *et al.* Low offset frequency 1/f flicker noise in spin-torque vortex oscillators. *Phys. Rev. B* **99**, 235135 (2019).
31. Quinsat, M. *et al.* Amplitude and phase noise of magnetic tunnel junction oscillators. *Appl. Phys. Lett.* **97**, 182507. https://doi.org/10.1063/1.3506901 (2010).
32. Grimaldi, E. *et al.* Response to noise of a vortex based spin transfer nano-oscillator. *Phys. Rev. B* **89**, 104404. https://doi.org/10.1103/PhysRevB.89.104404 (2014).
33. Kim, J.-V., Tiberkevich, V. & Slavin, A. N. Generation linewidth of an auto-oscillator with a nonlinear frequency shift: spin-torque nano-oscillator. *Phys. Rev. Lett.* **100**, 017207 (2008).
34. Silva, T. J. & Keller, M. W. Theory of thermally induced phase noise in spin torque oscillators for a high-symmetry case. *IEEE Trans. Magn.* **46**, 3555–3573 (2010).
35. Rubiola, E. *Phase Noise and Frequency Stability in Oscillators* (Cambridge University Press, Cambridge, 2008).
36. Diao, Z., Nowak, E. R., Haughey, K. M. & Coey, J. M. D. Nanoscale dissipation and magnetoresistive1/fnoise in spin valves. *Phys. Rev. B* **84**, 094412 (2011).
37. Nowak, E. R., Weissman, M. B. & Parkin, S. S. P. Electrical noise in hysteretic ferromagnet-insulator-ferromagnet tunnel junctions. *Appl. Phys. Lett.* **74**, 600–602 (1999).
38. Arakawa, T. *et al.* Low-frequency and shot noises in CoFeB/MgO/CoFeB magnetic tunneling junctions. *Phys. Rev. B* **86**, 224423 (2012).
39. Eklund, A. *et al.* Dependence of the colored frequency noise in spin torque oscillators on current and magnetic field. *Appl. Phys. Lett.* **104**, 092405 (2014).
40. Keller, M. W., Pufall, M. R., Rippard, W. H. & Silva, T. J. Nonwhite frequency noise in spin torque oscillators and its effect on spectral linewidth. *Phys. Rev. B* **82**, 054416 (2010).
41. Sanches, F. *et al.* Current-driven gyrotropic mode of a magnetic vortex as a nonisochronous auto-oscillator. *Phys. Rev. B* **89**, 140410 (2014).
42. Dussaux, A. *et al.* Large microwave generation from current-driven magnetic vortex oscillators in magnetic tunnel junctions. *Nat. Commun.* **1**, 1–6 (2010).
43. Iacocca, E., Heinonen, O., Muduli, P. K. & Åkerman, J. Generation linewidth of mode-hopping spin torque oscillators. *Phys. Rev. B* **89**, 054402 (2014).
44. Thiele, A. A. Steady-state motion of magnetic domains. *Phys. Rev. Lett.* **30**, 230–233. https://doi.org/10.1103/PhysRevLett.30.230 (1973).
45. Dussaux, A. *et al.* Field dependence of spin-transfer-induced vortex dynamics in the nonlinear regime. *Phys. Rev. B* **86**, 014402 (2012).
46. Khalsa, G., Stiles, M. D. & Grollier, J. Critical current and linewidth reduction in spin-torque nano-oscillators by delayed self-injection. *Appl. Phys. Lett.* **106**, 242402 (2015).
47. See Supplemental Material at http://address_by_publisher.com for details on the simulations and a discussion of the modelled generating noise. We also derive the relation between phase variance and phase noise and moreover between phase variance and signal autocorrelation.
48. Demir, A. Phase noise and timing jitter in oscillators with colored-noise sources. *IEEE Trans. Circuits Syst. I Fundam. Theory Appl.* **49**, 1782–1791 (2002).
49. Demir, A. Computing timing jitter from phase noise spectra for oscillators and phase-locked loops with white and $1/f$ noise. *IEEE Trans. Circuits Syst. I Regul. Pap.* **53**, 1869–1884 (2006).
50. Godone, A., Micalizio, S. & Levi, F. RF spectrum of a carrier with a random phase modulation of arbitrary slope. *Metrologia* **45**, 313–324 (2008).
51. Makdissi, A., Vernotte, F. & Clercq, E. Stability variances: a filter approach. *IEEE Trans. Ultrason. Ferroelectr. Freq. Control* **57**, 1011–1028 (2010).
52. Riley, W., Time, P. L. U. & Division, F. *Handbook of Frequency Stability Analysis*. NIST special publication (U.S. Department of Commerce, National Institute of Standards and Technology, 2008). https://www.nist.gov/publications/handbook-frequency-stability-analysis.
53. Tiberkevich, V. S., Slavin, A. N. & Kim, J.-V. Temperature dependence of nonlinear auto-oscillator linewidths: application to spin-torque nano-oscillators. *Phys. Rev. B* **78**, 092401 (2008).

Acknowledgements

S.W. acknowledges financial support from Labex FIRST-TF under contract number ANR-10-LABX-48-01. The work is supported by the French ANR project "SPINNET" ANR-18-CE24-0012.

Author contributions

S.W. and V.C. conceived the project. K.Y. and S.T. prepared the devices, with the help of H.K.; A.F. and S.Y.; S.W. performed the experimental noise and frequency spectrum characterization and analyzed the data with the help of V.C., U.E. and P.B.; P.T. with the help of S.W performed the simulations; P.T. and S.W. developped the modelling with the help from E.R., S.G. and D.C.; S.W. and V.C. prepared the manuscript and S.W.,J.G.,S.G., G.C.,E.R., V.C. discussed and contributed to the final manuscript.

Competing interests

The authors declare no competing interests.

Additional information

Supplementary information is available for this paper at https://doi.org/10.1038/s41598-020-70076-0.

Correspondence and requests for materials should be addressed to S.W.